Revue-IRS

Revue Internationale de la Recherche Scientifique (Revue-IRS)

ISSN: 2958-8413

Vol. 3, No. 6, Décembre 2025

This is an open access article under the CC BY-NC-ND license.

Spatio-temporal dynamics of the evolution of atmospheric pollutants in the itasy region

HERITAHINA Rambeloson[1,3], RASOLOMANANA Eddy Harilala [1,2], RANDRIANJA Kanto Volahasina[1,3]

[1]Ecole Doctorale Ingénierie et Géosciences, [2]Ecole Supérieure Polytechnique d'Antananarivo, [3]Université de l'Itasy

Abstract: This study aims to characterize the spatiotemporal dynamics of major pollutant gases—NO_2, CO, SO_2, O_3, and CH_4—in the Itasy region of Madagascar over the period 2019-2024, using Sentinel-5P/TROPOMI satellite data series. Monthly TROPOMI data were analyzed using statistical methods (nonparametric trend tests, correlations). The results show that CO and NO_2 exhibit strong seasonal variations, with peaks at the end of the dry season, such as CO increasing from approximately 0.021 to 0.037 mol/m² between February and October, and NO_2 from 9×10^{-6} to 2.3×10^{-5} mol/m². Tropospheric ozone follows a regular annual cycle, with a maximum (0.129 mol/m²) in October (dry season) and a minimum in May. Average SO_2 remains very low throughout the year (values close to zero). Spatially, CO, NO_2, and O_3 are more concentrated around urban centers and roads (Arivonimamo, Miarinarivo) than in rural areas. In addition, methane shows an upward trend from 1830 ppb in 2019 to 1875 ppb in 2024, an increase of +2.5%. These results confirm the strong seasonality of primary pollutants linked to anthropogenic activities such as vegetation fires, traffic, and weather conditions.

Keywords: Sentinel 5P image, atmospheric pollutants, time series, spatial correlation, meteorological parameters

Digital Object Identifier (DOI): https://doi.org/10.5281/zenodo.**17848032**

1 Introduction

The analysis of air quality in the Malagasy Highlands, more specifically in the Itasy region, is a relevant area of study for better understanding local atmospheric dynamics. The peri-urban and rural areas of Itasy are characterized by slash-and-burn farming, limited waste management, and informal activities such as brick making, which have been identified as major sources of atmospheric emissions. These factors contribute to worrying levels of air pollutants and significant spatial variability within the territory. [1] This local assessment is part of a national context in which climate change has become a major issue: Madagascar is one of the country's most vulnerable to climate change and least prepared to deal with it, which increases the risks associated with hazards (cyclones, droughts, floods) and environmental exposure. [2]

In this context, the period 2019-2024 is of particular scientific interest: it corresponds to the continuous availability of Sentinel-5P/TROPOMI satellite data, which enable the mapping and monitoring of the spatiotemporal dynamics of the main gas tracers in a predominantly rural area such as Itasy. [3]

This study, entitled "Spatiotemporal dynamics of atmospheric pollutant evolution in the Itasy region," has the overall objective of characterizing the spatiotemporal dynamics of major atmospheric pollutants—nitrogen dioxide (NO_2), carbon monoxide (CO), sulfur dioxide (SO_2), ozone (O_3), and methane (CH_4)—in the Itasy region, based on continuous satellite data series, in order to better understand the climate issues facing this territory.

In light of this, two working hypotheses are proposed. First hypothesis: In the Itasy region, NO_2 and CO concentrations vary greatly throughout the year, with increases expected during the dry season and during vegetation fires, which should be clearly visible in the Sentinel-5P/TROPOMI series. Second hypothesis: O_3 levels, and to a lesser extent SO_2 levels, change with the seasons, influenced by sunlight. Dry periods are particularly conducive to the formation of tropospheric ozone and the accumulation of gases that contribute to its production.

To better understand this, we will first review the materials and methods used, including the datasets and adopted methodology. Then, we will examine the results and interpretation of the characteristics of temporal variations in atmospheric pollutants, followed by their spatiotemporal variations and an analysis of temporal trends. In the discussion section, we will examine the correlation between meteorological factors and atmospheric pollutants, as well as the limitations and prospects of our research.

2 Materials and Methods

2.1 Study Area

The Itasy region, located in the center of Madagascar's highlands, covers an area of approximately 6,993 km². It is bordered to the north by the Analamanga region, to the west by Bongolava, to the south by Vakinankaratra, and to the east by Amoron'i Mania. Itasy is characterized by volcanic terrain with altitudes ranging from 950 to 1,300 m, and by the presence of Lake Itasy, a major water reservoir that supports fishing, irrigation, and tourism activities. [4] [5]

The region has a tropical highland climate, with hot, humid seasons and annual rainfall ranging from 1,330 to 1,575 mm, which, according to the Bank, directly influences the dispersion of air pollutants and the seasonal formation of tropospheric ozone (O_3). Traditional agricultural practices, such as biomass combustion and the burning of agricultural residues. The climate of the Highlands is characterized by a rainy season from November to March/April and a dry, cooler season from May to October, which imposes a strong seasonality on the atmospheric and hydrological processes observed in the study area. Antananarivo thus has a subtropical climate characterized by temperate (not too hot) summers. These climatic characteristics, confirmed by climatological summaries and monthly precipitation profiles, provide the framework for the spatio-temporal analysis of pollutants that the study proposes to conduct. [6]

Our study focuses on the Itasy region, specifically in the districts of Soavinandriana, Miarinarivo, and Arivonimamo. The following figure shows a map of the Itasy region.

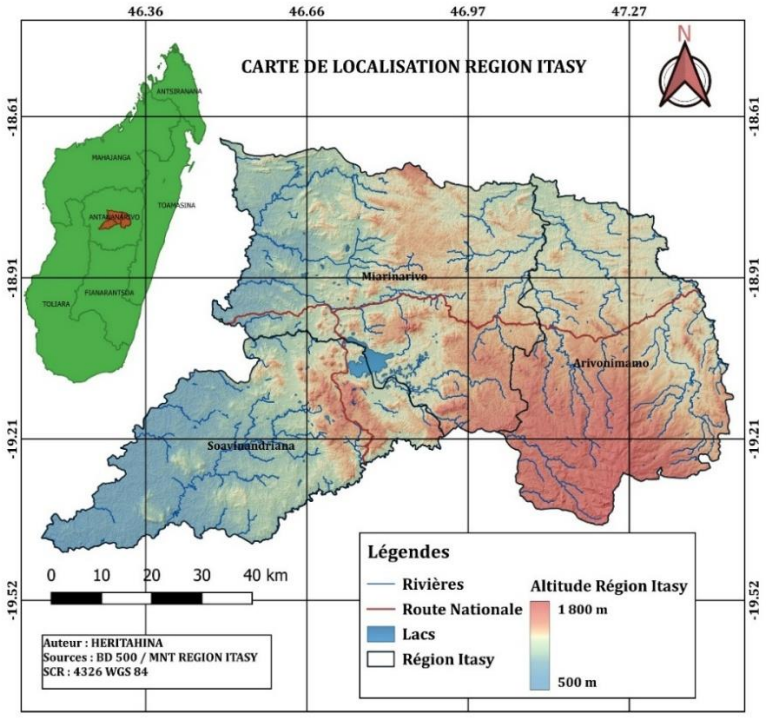

Figure 1. Map showing the location of the Itasy regions

2.2 Data set used

The data set includes all key data such as Sentinel-5P data sets and climate variability data.

2.2.1 Key data

The table below summarizes the Sentinel-5P/TROPOMI OFFL/L3 datasets used, as well as the unit, nominal resolution, and date of availability for each pollutant.

Table 1. Data used

Polluant	Earth Engine (ID & bande)	Unit	Resolution	Start of data
Nitrogen dioxide	COPERNICUS/S5P/OFFL/L3_NO2-Band :tropospheric_NO2_column_number_density	mol/m²	~1 113 m (0,01°)	June 28, 2018
Carbon monoxide	COPERNICUS/S5P/OFFL/L3_CO-Band : CO_column_number_density	mol/m²	~1 113 m (0,01°)	June 28, 2018
Sulfur dioxide	COPERNICUS/S5P/OFFL/L3_SO2-Band : SO2_column_number_density	mol/m²	~1 113 m (0,01°)	December 5, 2018
Ozone	COPERNICUS/S5P/OFFL/L3_O3-Band : O3_column_number_density	mol/m²	~1 113 m (0,01°)	September 8, 2018
Méthane	COPERNICUS/S5P/OFFL/L3_CH4 - Band :CH4_column_volume_mixing_ratio_dry_air	ppb/ppm	~1 113 m (0,01°)	February 8, 2019

2.2.2 Additional data

The table below summarizes the climate datasets used (CHIRPS v2) for precipitation (0.05° grid, 1981-present), ERA5 Monthly for temperature, and TerraClimate for monthly climate variables (1/24°, ~4 km, 1958-present), specifying for each the key variables, unit, resolution, and update period. [7]

Table 2. Additional datasets used

	Dataset	Key variables	Unit	Resolution	Start of data
Precipitations	**CHIRPS v2**	Precipitation	mm/j	0,05° (5,6 km)	1981
Temperature	**ERA5 Monthly**	mean_2m_air_temperature (T2m),	m/s	0,25° (31 km)	1979
Monthly climate	**TerraClimate**	tmin, tmax, ws (wind), ppt, vapor_pressure	°C	4 km (1/24°)	1958
Fire data	**MCD64A1**	MCD64A1 Burn Date (day of burning), derived burned area (pixelArea)	No unit, area in ha ($m^2/10^4$)	500 m (0,005°)	2000 (start of MODIS)

2.3 Data processing flowchart

The study area is defined by isolating the region from the GAUL level 1 (ADM1) administrative boundaries, which provides an official and consistent perimeter for all subsequent spatial aggregations. In parallel with geographic information system operations in QGIS (import, cartographic consistency checks, and layout), the Sentinel-5P/TROPOMI collections in OFFL/L3 mode are opened in Google Earth Engine in order to load the NO_2, CO, SO_2, O_3, and CH_4 gas tracers required for spatio-temporal analyses. The Earth Engine datasets describe, in particular, the OFFL/L3 NO_2 and OFFL/L3 CH_4 products, used here as references for the period 2019-2024.

The pre-processing applied in GEE includes a 2019-2024 temporal filter, a spatial filter on Itasy via filterBounds then clip, and the use of gridded L3 products that facilitate regular aggregation at the regional level.

Spatio-temporal aggregations are produced in the form of monthly and annual composites by pollutant and accompanied by zonal statistics calculated by region and district in order to quantify average levels, gradients, and intra-regional contrasts.

Visualization and analysis combine maps by pollutant and period with time series covering the entire study window, making it possible to identify hotspots, seasonality, and possible interannual anomalies.

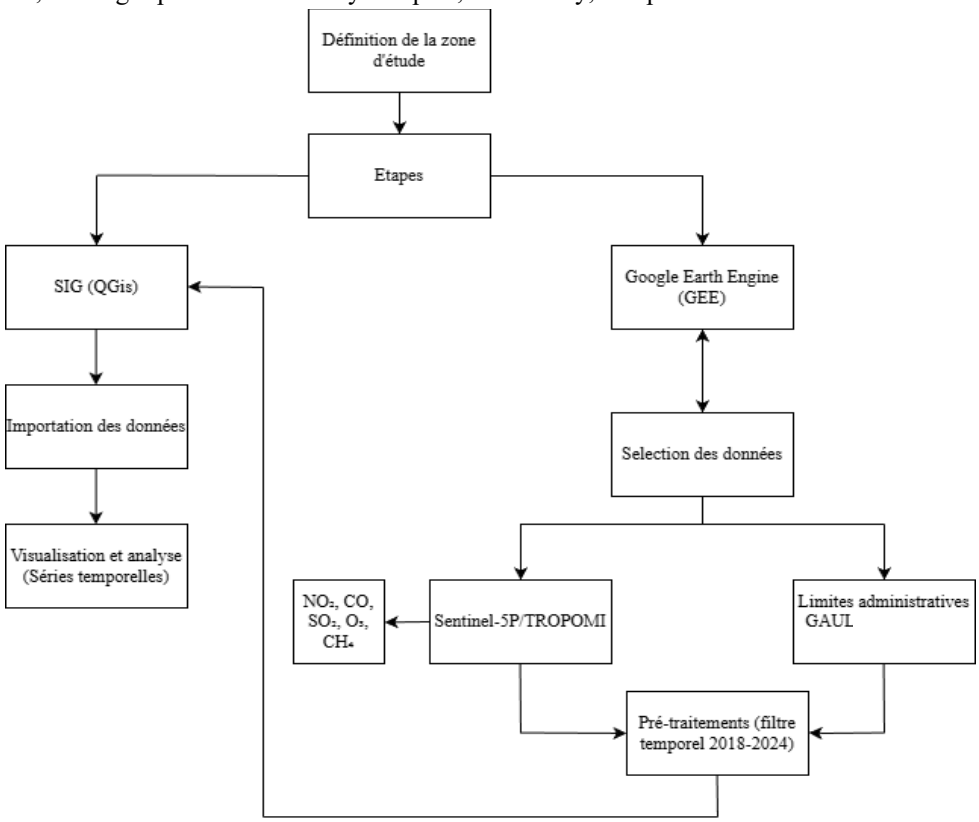

Figure 2. Data processing procedures

2.4 Methodology for analyzing monthly trends in pollutant concentrations using Mann-Kendall

To statistically evaluate monotonic trends in pollutant concentrations over time, we conducted the nonparametric Mann-Kendall (MK) trend test on the monthly average values of CO, NO_2, SO_2, and O_3 concentrations over the period 2019-2024. The Mann-Kendall test is widely used in the exploration of environmental time series because of its robustness to missing data, non-normal distributions, and the absence of linearity assumptions. The test was performed on the time series for each pollutant, yielding Kendall's τ coefficient, the p-value, and the trend class (increasing, decreasing, or no trend). A significance level of $\alpha = 0.05$ was used to assess statistical significance. This step was decisive in quantifying long-term changes in concentrations and validating the patterns observed in the spatiotemporal maps. The Mann-Kendall results were then cross-referenced with spatial analysis to visualize statistically significant trends and interpret the dynamics. [8]

2.4.1 Monthly series by pollutant and region

For a pollutant p (CO, NO_2, SO_2, O_3) and a region r, the series of monthly averages {x_t }_(t=1…n), the Mann Kendall statistic is written as:

$$S = \sum_{i=1}^{n-1} \sum_{j=i+1}^{n} sgn(x_j - x_i), \quad sgn(u) = \begin{cases} +1 & u > 0 \\ 0 & u = 0 \\ -1 & u < 0 \end{cases}$$

And Variance with correction for ties $(t_1, \ldots, t_g)$:

$$Var\ (S) = \frac{n(n-1)(2n+5) - \sum_{p=1}^{g} t_p(t_p-1)(2t_p+5)}{18}$$

The normalized statistic with continuity correction is:

$$Z = \begin{cases} \dfrac{S-1}{\sqrt{Var(S)}} & if\ S > 0, \\ 0 & if\ S = 0, \\ \dfrac{S+1}{\sqrt{Var(S)}} & if\ S < 0. \end{cases}$$

2.4.2 Seasonal Kendall Adaptation

Pollutants exhibit monthly seasonality (weather chemistry, burning cycles, heating, etc.). To avoid this, we apply the Seasonal Mann Kendall method for each month. $m \in \{1, \ldots, 12\}$ construct the interannual sub-series $\{x_{m,y}\}_{y=2019-2024}$, calculate S_m and $Var(S_m)$ as above, comparing only the same months (January with January, etc.), then aggregate [10]

$$S_{SK} = \sum_{m=1}^{12} S_m, \qquad Var\ (S_{SK}) = \sum_{m=1}^{12} Var(S_m)$$

2.4.3 Air-specific magnitude and interpretation

Kendall's tau: $\tau = S/\binom{n}{2}$ (or with Seasonal MK, τ is calculated from S_{SK} ummarizes the direction and strength of the trend (values close to ±1= clear trend). [6]

2.4.4 Pearson correlation

In order to analyze the linear relationships between the different variables considered (air pollutants and possibly meteorological parameters), a Pearson correlation matrix was calculated. This matrix groups together the correlation coefficients r that exist between all pairs of variables observed in a square table. Pearson's linear correlation coefficient, which can be calculated and understood for two quantitative variables, makes it possible to assess the intensity and direction of the linear relationship between them. [11]

For two variables X and Y, Pearson's correlation coefficient r_{XY} is defined by :

$$r_{XY} = \frac{\sum_{i=1}^{n}(x_i - \bar{x})(y_i - \bar{y})}{\sqrt{\sum_{i=1}^{n}(x_i - \bar{x})^2}\sqrt{\sum_{i=1}^{n}(y_i - \bar{y})^2}}$$

where x_i et y_i represent the observed values of variables X et Y, x and y their respective means, and n the number of observations. The coefficients r take values between -1 and +1. A value close to +1 indicates a strong positive linear correlation (the two variables tend to move in the same direction), a value close to -1 indicates a strong negative linear correlation (an increase in one is associated with a decrease in the other), while a value close to 0 suggests the absence of a marked linear relationship.

For this study, Pearson's correlation matrix was established based on the series of monthly averages for each year of the period under consideration. This approach makes it possible to identify pollutants that behave similarly over time, likely due to common emission sources or similar formation mechanisms, and to track the evolution of these relationships from one year to the next.

The correlation matrices obtained in this way are a diagnostic tool for understanding the signatures of sources and interactions between pollutants in the region under study. Pearson's correlation matrix R brings together all the coefficients r_{ij} between each pair of variables (pollutants, meteorological parameters).

$$R = \begin{pmatrix} 1 & r_{12} & \ldots & r_{1p} \\ r_{21} & 1 & \ldots & r_{2p} \\ \vdots & \vdots & \ddots & \vdots \\ r_{p1} & r_{p2} & \ldots & 1 \end{pmatrix}$$

2.4.5 Estimating the trend using Sen's slope

In order to quantify the magnitude of the trends identified by the Mann-Kendall test, we used Sen's slope estimator (Theil-Sen). This is a nonparametric method that provides a robust estimate of the linear trend in a time series. It is widely used in hydrology, climatology, and air quality studies because of its low sensitivity to outliers and non-normality of data [12].

For each air pollutant (CO, NO_2, SO_2, O_3, CH_4), the series of monthly averages x_t was considered over the study period. The Sen slope β is calculated as the median of all slopes between all pairs of points (t_i, x_i) et (t_j, x_j) with $j > i$:

$$\beta = median\left(\frac{x_j - x_i}{t_j - t_i}\right), \forall\, j > i.$$

A positive slope (β>0) indicates an upward trend in pollutant concentrations, while a negative slope (β<0) indicates a downward trend (relative improvement in air quality for that pollutant). The combination of the Mann-Kendall test (for the direction and significance of the trend) and Sen's slope (for the intensity of the trend) thus provides a robust characterization of the temporal evolution of air pollutants in the region studied. The estimated Sen slope values for each pollutant are then plotted graphically in order to visually compare the relative importance of trends between different pollutants and/or between different periods considered. [13]

3 RESULTS AND INTERPRETATION

3.1 Variation of meteorological parameters in the Itasy region between 2019 to 2024

The figure below illustrates the monthly evolution of the main meteorological parameters in the Itasy region, with the observed series shown as a solid line and a smoothed curve shown as a dotted line for each variable. The alternation between the rainy season and the dry season typical of the tropical highland climate is clearly visible.

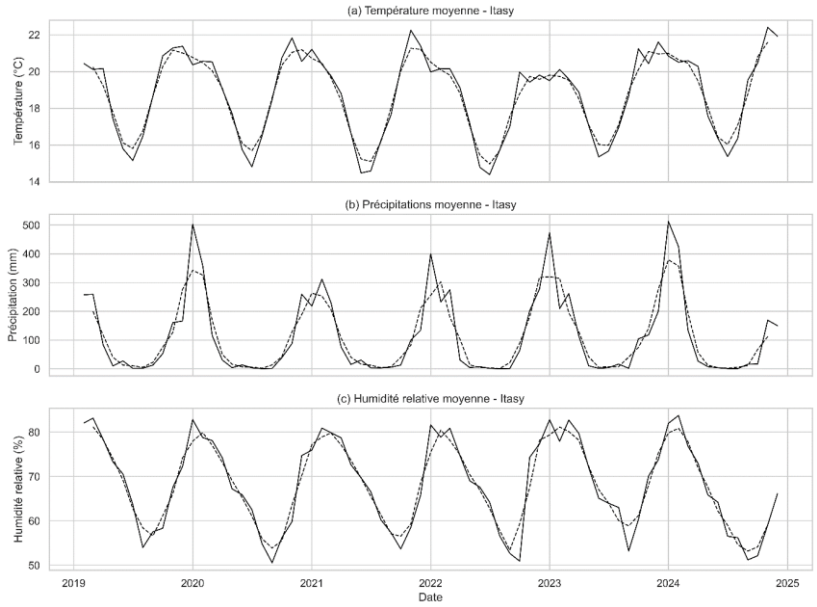

Figure 1. Variation in meteorological parameters in the Itasy region: (a) average temperature, (b) average precipitation, and (c) average relative humidity

(a) Average temperature

The average temperature generally ranges between 15°C and 22°C. Each year, a maximum is observed between November and March, when temperatures regularly exceed 20-21°C, followed by a marked minimum during the cool, dry season from June to September, around 15-16°C. From one year to the next, variations are moderate: the temperature regime remains relatively stable, with only slight differences in the intensity of the maximum and minimum temperatures, confirming a fairly consistent climate on an interannual scale.

(b) Average precipitation

Precipitation shows a very contrasting seasonal cycle. The rainy season is concentrated each year between approximately November and March, with peaks that can exceed 400-500 mm/month (particularly around the beginning of 2020 and 2024), reflecting very intense rainfall events. Conversely, the dry season (mainly from June to September) is almost completely rainless, with monthly totals close to 0 mm. There are interannual differences: some rainy seasons are more pronounced (very heavy rainfall), while other years have slightly more moderate peaks, suggesting more or less humid seasons.

(c) Average relative humidity

Relative humidity logically follows rainfall patterns: the highest values (above 80%) occur during the rainy season, when precipitation is abundant and the atmosphere is more humid. In the dry season, relative humidity decreases significantly, falling to around 55-60%, reflecting drier air during cooler periods. Wet years result in higher or more sustained humidity plateaus, while slightly drier years show slightly lower values and more pronounced minimums.

3.2 Characteristics of temporal variations in atmospheric pollutants in the Itasy region

In this section, we present the variation curves between 2019 and 2024 for the main atmospheric pollutants studied (CH_4, C, NO_2, O_3, and SO_2), in order to characterize the spatio-temporal dynamics of air pollution in the Itasy region.

In general, the respective variations in CO, NO_2, SO_2, CH_4, and O_3 above the Itasy region tend to be explained by a similar set of probable causes, which are, on the one hand, anthropogenic emissions from fuel combustion in road traffic, older vehicles, generators, and certain small industries, all of which are likely to be significant sources of CO, NO_2, and SO_2; and, on the other hand, the widespread use of solid biomass and charcoal for cooking and domestic heating in Madagascar, as well as the burning of waste, which together account for the majority of CO, NO_2, SO_2, and VOCs, while methane (CH_4) comes from agricultural activities (flooded rice cultivation, livestock farming, organic waste management) and natural wetlands, which are known to be significant sources of CH_4 in tropical areas. Finally, Tropospheric ozone (O_3), which is formed by a series of photochemical reactions involving NO_x, CO, and VOCs under conditions of strong sunlight, according to well-established mechanisms, means that any increase in these precursors, NOx, CO, and VOCs under the synergy of weather conditions during the dry season causes a sharp increase in O_3 production in the atmospheric column.

3.2.1 CH_4 variation between 2019 to 2024

The following figure highlights an overall upward trend in methane (CH_4) over the entire 2019-2024 period. The annual average rises from around 1,830 ppb in 2019 to 1,875 ppb in 2024, an increase of around 45 units (2.5%), reflecting moderate seasonality but a gradual increase in background methane levels above the Itasy region.

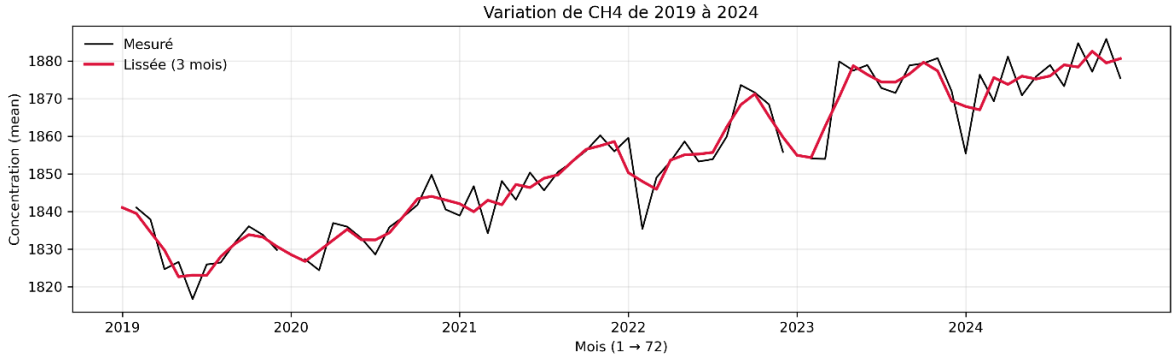

Figure 2. CH4 variation between 2019 to 2024

3.2.2 CO variation between 2019 to 2024

For carbon monoxide (CO), the figure highlights strong seasonal cyclicality. On average, the lowest values are observed in February, at around 0.021 mol/m², while the maximum values reach around 0.037 mol/m² in October. Over the entire 2019-2024 period, monthly concentrations range from 0.019 to 0.046 mol/m², with an annual average rising from around 0.025 mol/m² in 2019 to 0.028 mol/m² in 2024 (an increase of around 14%). These values confirm the existence of marked peaks at the end of the dry season/beginning of the hot season.

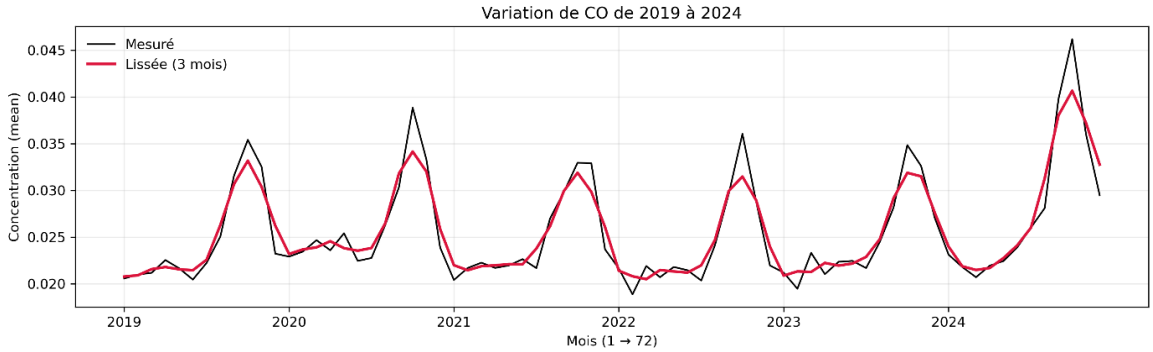

Figure 3. CO variation between 2019 to 2024

3.2.3 NO2 variation between 2019 to 2024

Nitrogen dioxide (NO_2) in mol/m² also shows a clear seasonal cycle. Average monthly values increase from 9×10^{-6} (minimum in February) to 2.3×10^{-5} (maximum in September). Over the period studied, concentrations generally ranged between 8×10^{-6} and 2.8×10^{-5}, with an average of 1.3×10^{-5}. The annual average rose from around 1.3×10^{-5} in 2019 to 1.5×10^{-5} in 2024, representing an increase of around 14% and indicating an increasingly significant NO_2 load in the atmospheric column, probably linked to the increase in anthropogenic emissions.

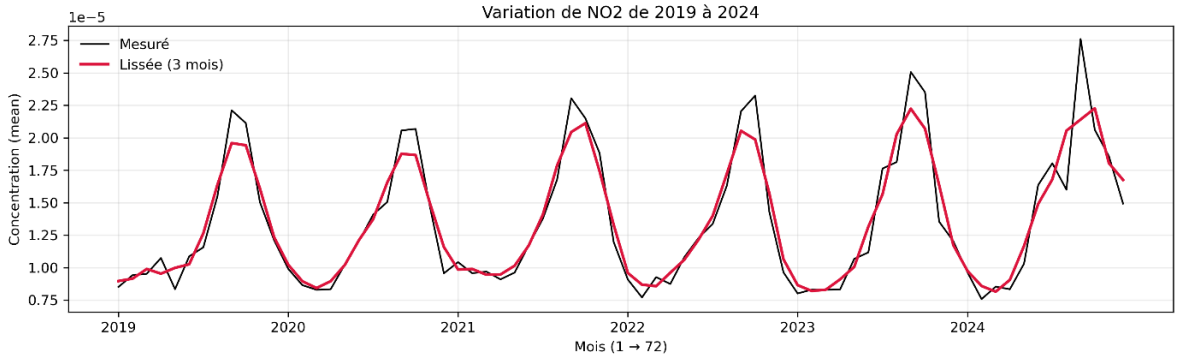

Figure 4. NO2 variation between 2019 to 2024

3.2.4 O3 variation between 2019 to 2024

The ozone (O_3) series in mol/m² shows almost regular seasonal variability. Monthly averages range from approximately 0.113 (minimum in May) to 0.129 (maximum in October). Over the entire period from 2019 to 2024, concentrations range from 0.111 mol/m² to 0.133 mol/m², with an average rate of around 0.120 mol/m². Annual averages are relatively stable (0.118 in 2019 and 0.118 in 2024), with slightly higher years (0.122 in 2021-2023), suggesting interannual variability in ozone peaks rather than a marked upward trend.

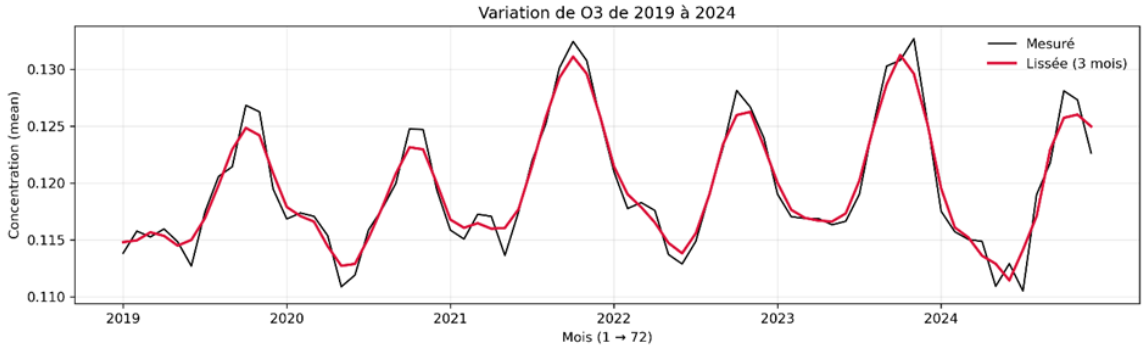

Figure 7. O_3 variation between 2019 to 2024

3.2.5 SO2 variation between 2019 to 2024

Finally, for sulfur dioxide (SO_2) at very low levels, monthly values generally range between -5.4×10^{-5} and 1.35×10^{-4} for an overall average close to 1.4×10^{-5}, with an average minimum observed in April (-3.1×10^{-5}) and an average maximum observed in July (7.9×10^{-5}). Annual averages remain close to zero (from -2×10^{-6} in 2019 to 1.1×10^{-5} in 2024), confirming the very low background concentration of SO_2 in Itasy.

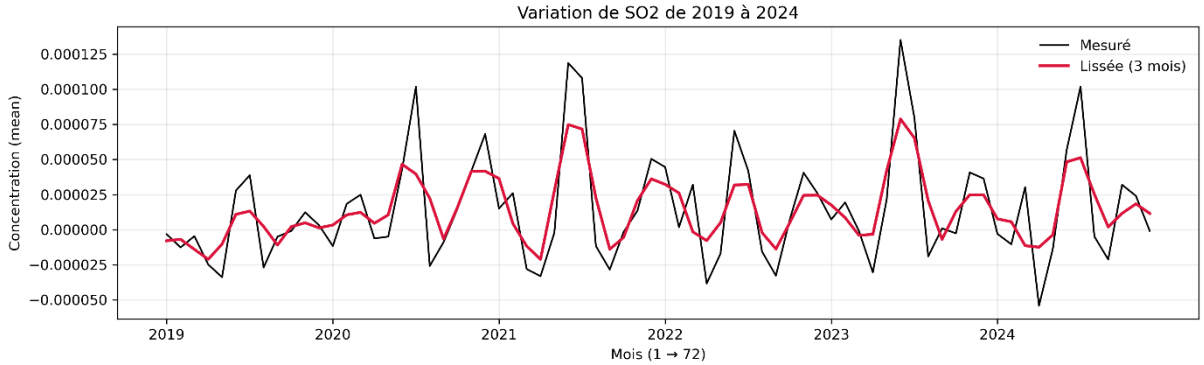

Figure 5. SO2 variation between 2019 to 2024

3.3 Spatiotemporal variation of atmospheric pollutants in the Itasy region

The following figure shows the average spatial distribution of the main atmospheric pollutants (CH_4, CO, NO_2, O_3, and SO_2) over the period 2019-2024 in the Itasy region, highlighting the contrasts between the districts of Miarinarivo, Soavinandriana, and Arivonimamo.

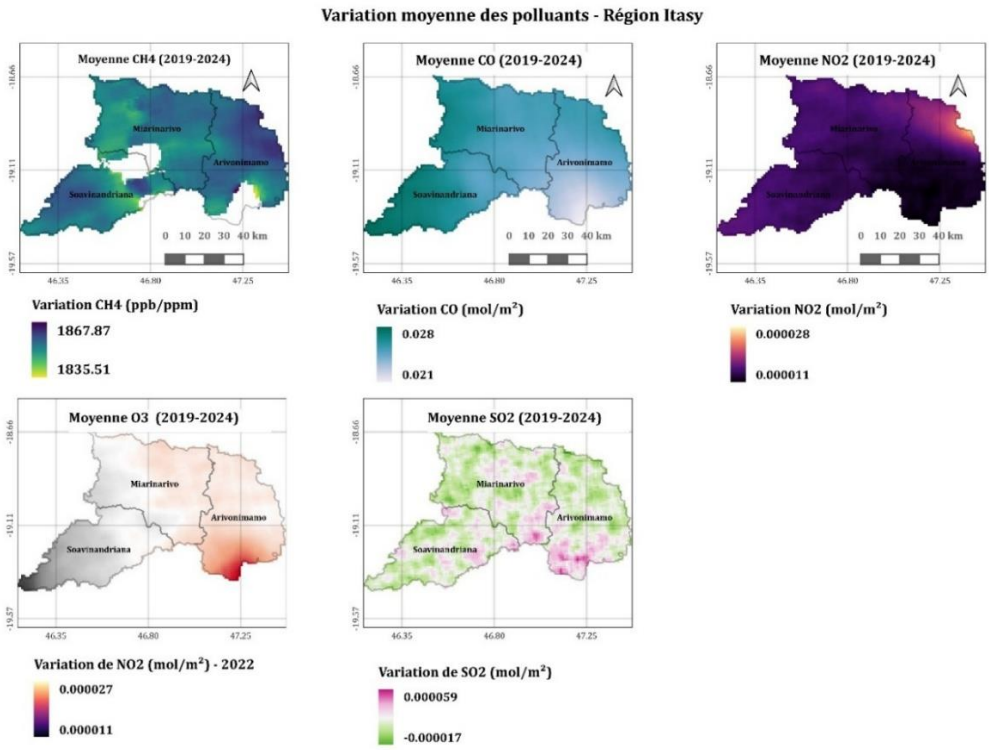

Figure 9. Average variation in air pollutants between 2019 to 2024

Generally, the maps show that average pollutant concentrations are not uniform across the region, but exhibit spatial gradients related to population density, transportation corridors, and certain local environmental characteristics.

CH_4 (2019-2024): Average methane values range from approximately 1835 to 1868 ppb/ppm, with generally higher levels in the northeastern and eastern parts of the region, near Arivonimamo and more anthropized areas, while slightly lower values are observed in the southwest, around Soavinandriana. This distribution may be associated with a combination of agricultural activities (flooded rice cultivation, livestock farming) and the presence of wetlands, which promote CH_4 emissions.

CO (2019-2024): carbon monoxide has average values between 0.021 to 0.028 mol/m², with a gradient indicating slightly higher levels around Arivonimamo and Miarinarivo, where roads and urban centers are concentrated, and lower values in the more rural areas of Soavinandriana. This suggests that road traffic, domestic combustion, and biomass fires play an important role in the distribution of CO.

NO_2 (2019-2024): The NO_2 map clearly shows a hotspot of higher concentrations in the east of the region, particularly around Arivonimamo, with average values ranging from 1.1×10^{-5} to 2.8×10^{-5} mol/m². This area corresponds to the vicinity of the axis connecting Itasy to Antananarivo and to more urbanized areas, suggesting a marked influence of road traffic, combustion activities, and population density. Levels are lower in the west and south (Soavinandriana).

O_3 (2019-2024): For ozone, average values also increase towards the extreme southeast of the region, where concentrations are higher near Arivonimamo, while lower values are observed towards the center and west. This pattern is consistent with the fact that O_3 is a secondary pollutant, formed from precursors (NO_x, CO, VOCs) emitted in more anthropized areas; the presence of higher ozone levels in these areas therefore reflects photochemical production from precursor gases.

SO_2 (2019-2024): sulfur dioxide concentrations are very low, with a map marked by a mosaic of small patches of positive and negative values, with no clear hot spots. This indicates that the average SO_2 load remains low overall across the Itasy region, with any contributions likely coming from point sources of sulfur fuel

combustion (diesel, fuel oil, generators, waste burning) and episodic regional contributions, without a marked spatial structure as for NO_2 or CO.

These results show that the most anthropized areas with the best road network connections (especially around Arivonimamo and Miarinarivo) have the highest levels of primary pollutants (CO, NO_2) and ozone, while more rural areas, particularly around Soavinandriana, generally have lower levels, with the exception of gases linked to natural processes such as CH_4.

3.4 Analysis of temporal trends

In order to characterize the temporal evolution of the main atmospheric pollutants above the Itasy region over the period 2019-2024, we applied the nonparametric Mann-Kendall test to the monthly TROPOMI series, supplemented by the Sen slope estimate (average variation per month and per year). The table below summarizes this nonparametric Mann-Kendall test.

Table 2. Mann Kendall nonparametric test and Sen slope

Polluants	Tau	P value	Trend	Sen slope per month	Sen slope per year	Lin slope per month visual
CH4	0.742540	0.000000	increasing	8.863108e-01	1.063573e+01	8.438693e-01
NO2	0.123631	0.125697	no trend	3.879359e-08	4.655231e-07	5.294121e-08
CO	0.115806	0.151553	no trend	2.584303e-05	3.101164e-04	5.663087e-05
O3	0.120501	0.135594	no trend	4.613627e-05	5.536352e-04	5.254680e-05
SO2	0.079030	0.328514	no trend	1.701011e-07	2.041213e-06	2.142456e-07

From a statistical point of view, the results clearly highlight contrasting behavior between methane and other pollutants. CH_4 has a Kendall coefficient $\tau = 0.74$ with a p-value < 0.001, indicating a strongly increasing and highly significant monotonic trend. The Sen slope is +0.89 units per month, or approximately +10.6 units per year, consistent with the linear regression line (+0.84 units/month). Conversely, NO_2, CO, O_3, and SO_2 are characterized by low τ values ($0.08 \leq \tau \leq 0.12$) and p-values greater than 0.10, leading to the conclusion that there is no significant monotonic trend for these species. Their annual Sen slopes remain very low (less than 6×10^{-4} units/year), confirming that, despite high seasonal variability, their average levels did not significantly increase or decrease over the 2019-2024 period in Itasy.

The figure above illustrates, for each pollutant, the raw monthly series, the smoothed series (3 month moving window), and the associated trend lines.

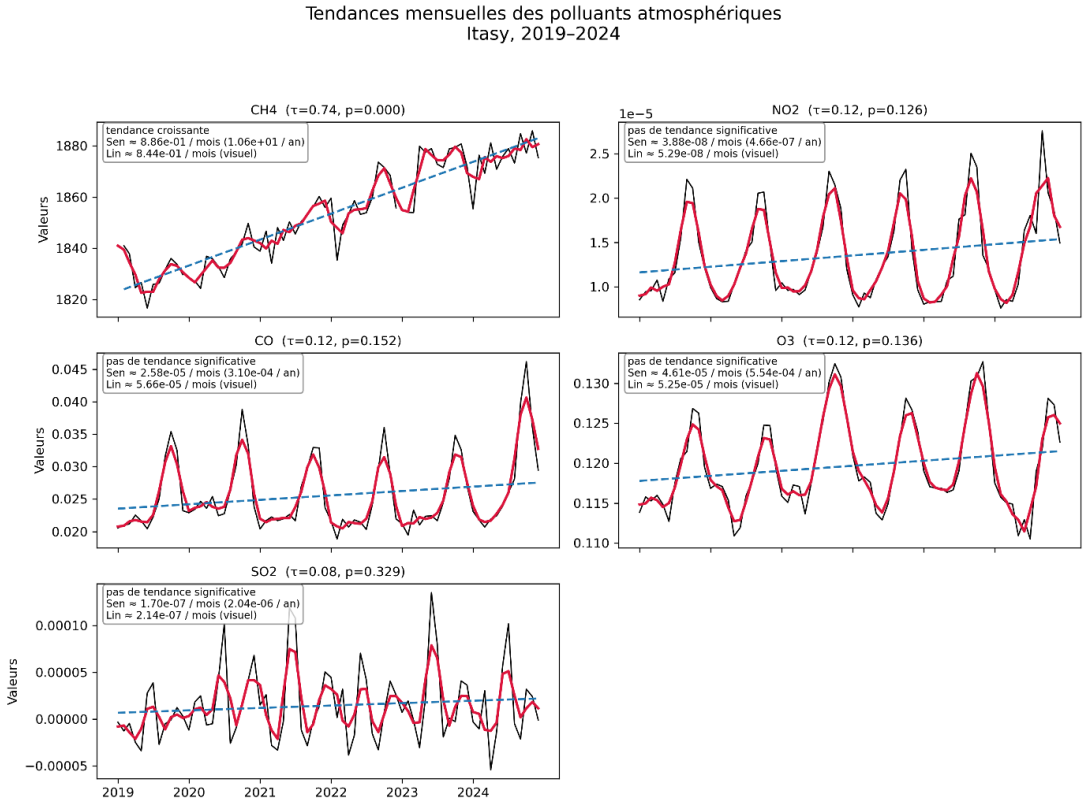

Figure 6. Monthly trends in air pollutants

The Mann-Kendall test applied to the monthly series for 2019-2024 shows very contrasting behaviors depending on the pollutant. For NO_2, CO, O_3, and SO_2, the Kendall coefficients are low and positive ($\tau = 0.12$ for NO_2, 0.12 for CO, 0.12 for O_3, and 0.08 for SO_2) with p-values between 0.13 and 0.33. These values indicate a slightly increasing but non-significant rank correlation at the 5% threshold, meaning that no sustained monotonic trend can be identified for these four pollutants over the period 2019-2024. Conversely, methane (CH_4) has a $\tau = 0.74$ with $p < 0.001$, reflecting a strongly increasing and statistically very significant monotonic trend. In other words, the order of monthly CH_4 concentrations consistently follows the chronological order: the closer we get to 2024, the higher the CH_4 levels.

3.5 Distribution of average pollutant concentrations

The following figure shows the distribution of average concentrations from 2019 to 2024 by pixel density of Sentinel 5P Tropomi satellite images.

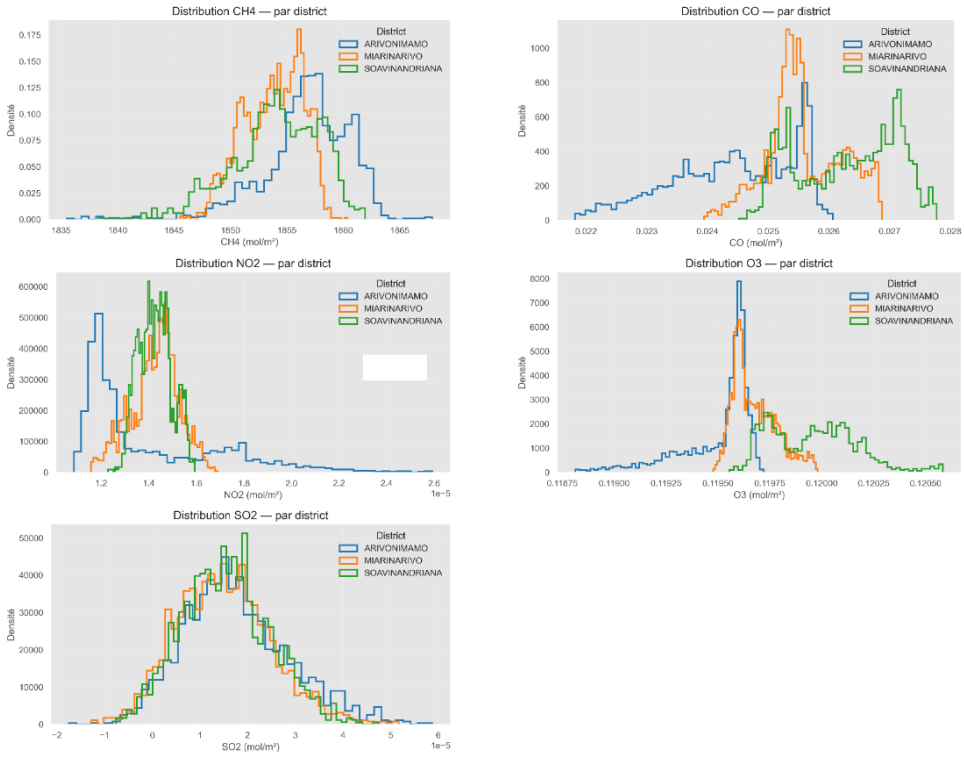

On the one hand, analysis of concentration distributions by district (Arivonimamo, Miarinarivo, and Soavinandriana) reveals broadly similar profiles, but with systemic contrasts depending on the pollutant. For SO_2, the histograms show very similar quasi-Gaussian shapes, centered around comparable values, implying relatively homogeneous background levels and combustion sources (wood or fuel-based) diffusely distributed throughout the region. The same is true for tropospheric ozone (O_3), which shows narrow distributions that overlap significantly between districts, with only a slight shift towards slightly higher values in Soavinandriana, indicating relatively uniform regional photochemical production and weak spatial gradients.

On the other hand, for carbon monoxide (CO), nitrogen dioxide (NO_2), and methane (CH_4), the difference is more pronounced. For CO, the distributions gradually shift from Arivonimamo (the lowest) to Soavinandriana (the highest), suggesting that the latter district has a systematically higher CO load, closely linked to more intense biomass combustion (slash-and-burn agriculture, domestic cooking) in rural areas. For NO_2, the variability in Arivonimamo is more pronounced, with the tail of the distribution extending to higher concentrations compared to Miarinarivo and Soavinandriana, which may reflect a more direct influence of roads and traffic emissions. Finally, CH_4 shows very distinct distributions between districts: Miarinarivo has a peak around concentrations that are again high but narrow, Arivonimamo shows higher, more spread-out average values, while Soavinandriana is slightly shifted towards lower levels. This spatial gradient suggests different contributions from biogenic sources of methane (irrigated rice fields, wetlands, livestock farming) from one district to another, in line with local contrasts in land use and agricultural practices.**Figure 7**. Distribution of average pollutant concentrations by district

4 Discussions

4.1 Spatial correlation between meteorological parameters and atmospheric pollutants over the period 2019 to 2024

The following figure illustrates the correlation matrix between meteorological parameters (temperature, precipitation, relative humidity), burned area, and atmospheric pollutants (CO, CH_4, O_3, SO_2, NO_2).

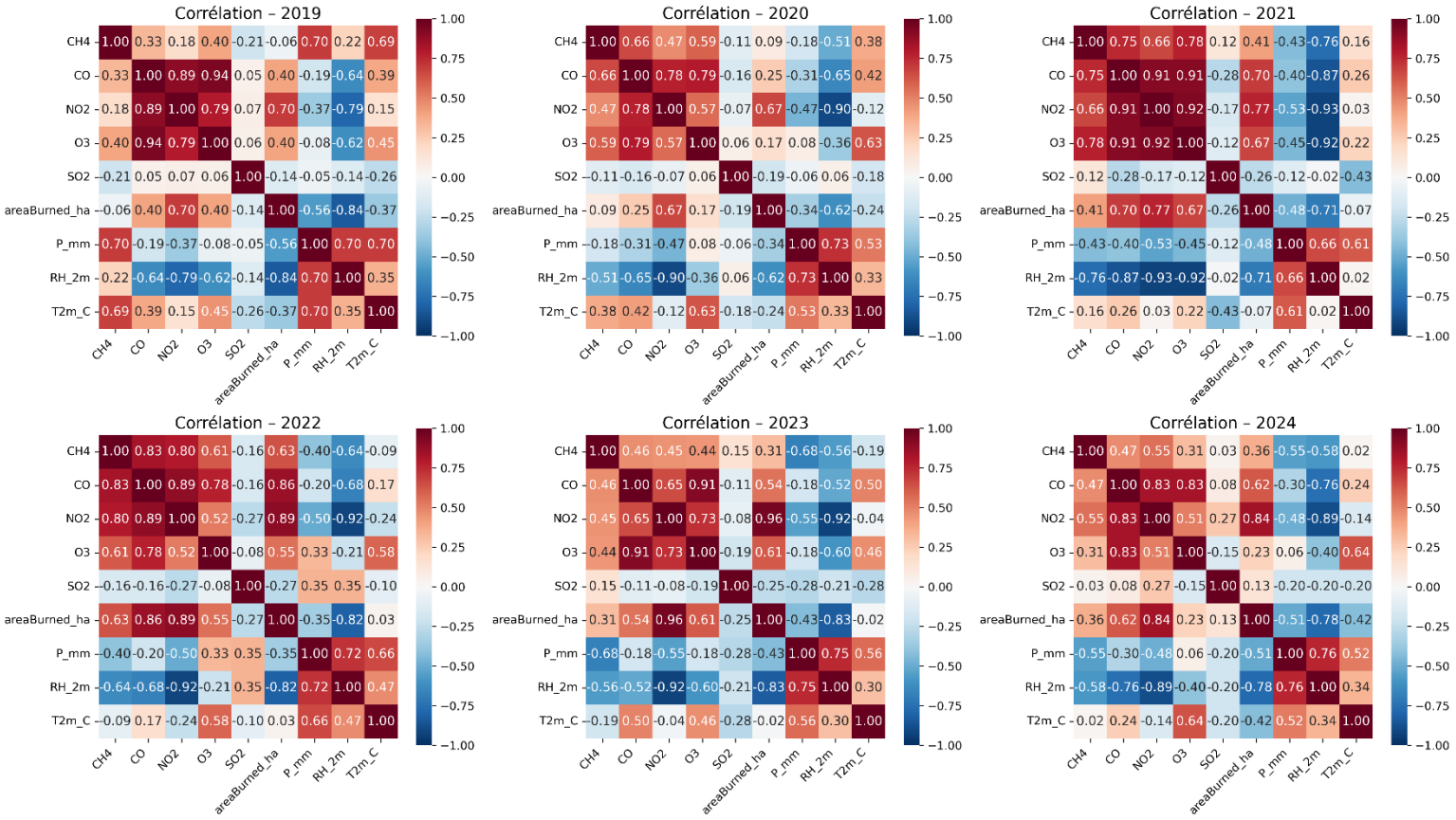

Figure 12. Correlation between meteorological parameters and air pollutants by year

Each annual correlation matrix reveals a consistent pattern. In general, variables related to drought (low precipitation or low humidity) are strongly correlated with large burned areas, while pollutants from combustion (CH_4, CO, NO_x, etc.) show high positive correlations between themselves and with fires.

Pearson's correlation matrix reveals significant relationships between meteorological variables, burned areas, and atmospheric pollutant concentrations during the period 2019-2024.

In 2019, precipitation and relative humidity were strongly correlated (r = 0.7) and showed a marked negative correlation with burned areas (up to r = -0.84). This indicates that fires develop mainly during dry periods, when vegetation dries out and becomes highly flammable fuel. Conversely, burned areas are positively correlated with NO_2, CO, and O_3 (r = 0.4-0.7), reflecting the increase in these pollutants linked to biomass fires and the photochemical formation of ozone from gases emitted during combustion: in practice, agricultural burning, bush fires, and intensive use of charcoal release large amounts of CO and NO_2, which then fuel O_3 production under the effect of solar radiation. CH_4 is mainly linked to the warm, wet season, with positive correlations with precipitation and temperature. This indicates a predominance of wet biogenic sources rather than fires, particularly flooded rice fields, marshy areas, and waterlogged soils rich in decomposing organic matter. Finally, SO_2 shows little correlation with other variables, suggesting that it mainly originates from emissions independent of seasonal fire dynamics and weather conditions. In rural areas, this may include activities such as traditional charcoal production, burning of agricultural or household waste, use of generators running on poor-quality diesel fuel, or, more locally, possible volcanic emissions.

In 2020, the strong correlation between precipitation and relative humidity (r = 0.73) and their positive links with temperature (r = 0.33-0.53) indicate a hot and humid season. However, these conditions are inversely related to burned areas (r = -0.34 to -0.62), showing that fires occur mainly during dry periods, when dry vegetation and agricultural residues promote their rapid spread. Relative humidity is strongly negatively correlated with combustion pollutants, particularly NO_2 (r = -0.90) and CO (r = -0.65), reflecting the scarcity of bushfires and agricultural burning during the wet season and the effect of rain leaching. During the dry season, CO, NO_2, and O_3 increase (CO-NO_2: r = 0.78; CO-O_3: r = 0.79; NO_2-O_3: r = 0.57), reflecting the impact of biomass fires and charcoal cooking, which are the main sources of air pollution in rural areas, emitting fine particles, CO, and volatile organic compounds (VOCs). Road traffic, which is generally light, contributes to a lesser extent to NOx, CO, and particle emissions. In addition, photochemical reactions can form tropospheric ozone, mainly from pollutants transported from urban areas, which can affect respiratory health and local ecosystems. Burnt areas are strongly correlated with NO_2 (r = 0.67), confirming that fires and burning are a major source of nitrogen oxides (NO and NO_2) in the region. CH_4 shows moderate correlations with temperature (r = 0.38) and with combustion pollutants (CO: r = 0.66; O_3: r = 0.59; NO_2: r = 0.47), indicating the combined influence of seasonal biogenic sources and human inputs. In contrast, SO_2 shows weak correlations (-0.19 to 0.06), suggesting that it comes from point or localized sources, such as the use of sulfur-containing fuels, certain industrial facilities, or volcanic emissions. Unlike NO_2 or CH_4, its concentrations do not vary significantly with the seasons or with the intensity of fires and climatic conditions, indicating less dependence on seasonal factors.

In 2021, climate variables remain interlinked, with a positive correlation between precipitation and relative humidity (P_mm and RH_percent: r = 0.66) and between precipitation and average temperature (P_mm and Tmean_C: r = 0.61), reflecting a hot and humid rainy season, while the link between RH_percent and Tmean_C is almost zero (r = 0.02). The areas burned are strongly negatively correlated with humidity (r = -0.71) and moderately correlated with rainfall (r = -0.48), indicating that bushfires and agricultural burning occur mainly during the dry season. These episodes are accompanied by a notable increase in pollutants: CH_4 (r = 0.41), CO (r = 0.70), NO_2 (r = 0.77), and O_3 (r = 0.67), reflecting the direct influence of biomass burning and atmospheric chemical reactions producing ozone. The correlations between pollutants are particularly strong (CO and NO_2: r = 0.91; CO and O_3: r = 0.91; NO_2 and O_3: r = 0.92; CH_4 and CO: r = 0.75; CH_4 and O_3: r = 0.78; CH_4 and NO_2: r = 0.66), revealing periods of pollution where several types of pollutants accumulate simultaneously, with emissions from fires, traffic, and charcoal cooking combining, and sunlight promoting ozone formation. Methane (CH_4) appears to be more synchronized with combustion pollutants than in previous years, suggesting that, in addition to wet biogenic sources (rice fields, wetlands), contributions from burning and human activities are contributing more to the signal. Finally, SO_2 remains weakly correlated with other variables (-0.43 to 0.12), indicating point or specific sources that are less influenced by seasonality and fire dynamics.

In 2022, meteorological variables remain strongly interrelated, with a positive correlation between precipitation and relative humidity (P_mm and RH_percent: r = 0.72) and between precipitation and average temperature (P_mm and Tmean_C: r = 0.66; RH_percent and Tmean_C: r = 0.47), reflecting a warm and humid rainy season, as is typically observed in the region. The areas burned are strongly negatively correlated with humidity (RH_percent and areaBurned_ha: r = -0.82) and moderately correlated with precipitation (P_mm and areaBurned_ha: r = -0.35), showing that large bushfires and agricultural burning occur mainly during very dry periods. During periods of drought, burned areas are strongly correlated with pollutants from combustion: CO (r = 0.86), NO_2 (r = 0.89), and O_3 (r = 0.55). This reflects the direct impact of agricultural fires, the use of solid fuels for cooking, and vehicle emissions on air quality, as well as the formation of ozone in the atmosphere from nitrogen oxides and carbon compounds under the action of sunlight. The concentrations of the various pollutants are strongly correlated (CO and NO_2: r = 0.89; CO and O_3: r = 0.78; NO_2 and O_3: r = 0.52), reflecting episodes where several pollutants accumulate simultaneously during peak fire periods. Compared to previous years, CH_4 appears to be more closely linked to this combustion dynamic (areaBurned_ha and CH_4: r = 0.63; CH_4 and CO: r = 0.83; CH_4 and NO_2: r = 0.80; CH_4 and O_3: r = 0.61), while remaining negatively correlated with precipitation and humidity (P_mm and CH_4: r = -0.40; RH_percent and CH_4: r = -0.64). This suggests that, in addition to traditional biogenic sources (rice fields, wetlands), fires and human activities contribute significantly to the CH_4 signal in 2022. Finally, as in previous years, SO_2 remains weakly correlated with other variables (coefficients between -0.27 and 0.35), indicating that it is not very sensitive to seasonal variations and the extent of burned areas.

In 2023, precipitation is negatively correlated with burned areas (P_mm and areaBurned: r = -0.43) and most pollutants, particularly CH_4 (r = -0.68) and NO_2 (r = -0.55), indicating that episodes of high pollution occur mainly during dry periods, when bushfires, agricultural burning, and charcoal stoves are most active. The burned areas also show an extremely strong correlation with NO_2 (areaBurned and NO_2: r = 0.96) and a high correlation with CO (r = 0.54) and O_3 (r = 0.61), as well as a moderate correlation with CH_4 (r = 0.31): this pattern reflects the direct impact of biomass combustion and the photochemical formation of ozone from nitrogen and carbon precursors emitted by fires. The pollutants themselves are strongly linked, with, for example, CO and O_3: r = 0.91, NO_2 and O_3: r = 0.73, CO and NO_2: r = 0.65, and significant correlations between CH_4 and CO, NO_2, and O_3 (r

between 0.44-0.46), reflecting episodes of multi-pollutant pollution combining smoke from fires, domestic emissions (cooking, heating), and road traffic. SO_2, on the other hand, remains weakly correlated with the other variables (coefficients between -0.28 and 0.15).

In 2024, precipitation is strongly negatively correlated with burned areas (P_mm and areaBurned: r = -0.51) as well as with CH_4 (r = -0.55), NO_2 (r = -0.48) and, to a lesser extent, CO (r = -0.30), indicating that episodes of high pollution occur during dry periods, when grasses, savannas, and crop residues are highly flammable and bushfires and agricultural burning are intensive. The areas burned are strongly correlated with NO_2 (r = 0.84) and CO (r = 0.62), and more moderately with CH_4 (r = 0.36) and O_3 (r = 0.23), reflecting the direct impact of biomass combustion and human activities (slash-and-burn, charcoal cooking, road traffic) on air quality, as well as the formation of ozone in the atmosphere from nitrogen and carbon compounds emitted by fires. The pollutants are strongly correlated: CO-NO_2 (r = 0.83), CO-O_3 (r = 0.83), NO_2-O_3 (r = 0.51), and CH_4-NO_2 (r = 0.55; CH_4-CO: r = 0.47), reflecting episodes where several pollutants accumulate simultaneously, typical of burning seasons, when smoke from fires, domestic emissions, and traffic combine under strong sunlight to produce tropospheric ozone. SO_2 remains weakly correlated with other variables (-0.20 to 0.27), which means that it comes from point or localized sources.

4.2 Analysis of results in light of hypothesis

In order to better understand the mechanisms governing solar gas variability in Itasy, it is essential to refer to the initial expectations. This section will therefore assess the extent to which the trends observed for NO_2, CO, O_3, and SO_2 corroborate or, on the contrary, refute the expectations formulated in the introduction to our study.

Response to the first hypothesis: The Sentinel-5P series confirm that, in Itasy, NO_2 and CO vary significantly throughout the year, with peaks during the dry season. Annual data show that CO reaches its maximum (0.037 mol/m²) around October, while it is lowest (0.021 mol/m²) in February (wet season). Similarly, NO_2 rises from around 9×10^{-6} mol/m² in February to 2.3×10^{-5} mol/m² in September. These peaks coincide with episodes of vegetation fires and road traffic. In short, this hypothesis is validated: the dry season and burning lead to marked increases in NO_2 and CO. However, the trend test shows that there is no significant linear upward trend for NO_2 or CO over 2019-2024, indicating that these increases are related to seasonal variability rather than a continuous intensification of emissions.

Response to the second hypothesis: O_3 and SO_2 levels are indeed influenced by seasonality and sunshine. Tropospheric ozone has a characteristic annual cycle, with a minimum (0.113 mol/m²) in May and a peak (0.129 mol/m²) in October. This variation corresponds to the hypothesis: the dry season, which is sunnier, promotes the photochemical formation of O_3 from precursors (NO_x, CO). In contrast, SO_2 remains very low overall throughout the year and does not show any pronounced seasonal peaks. The weak seasonal correlations of SO_2 suggest that its sources (sulfur-containing fuels, small local industries) are sporadic and not very sensitive to seasonal cycles, unlike ozone. Thus, ozone clearly shows the expected dependence on climate and precursors, while SO_2, due to its low concentrations, does not appear to be a major factor in the production of tropospheric ozone in Itasy.

4.3 Limitations and perspectives of the study

Several limitations should be highlighted in this research on the spatio-temporal dynamics of atmospheric pollutant evolution in the Itasy region. First, the analysis is based mainly on Sentinel-5P/TROPOMI satellite data, aggregated at a fairly large spatial scale. Although these products are suitable for a regional perspective, they are not capable of accurately capturing local disparities (impact of villages, roads, small industrial areas, domestic combustion points, etc.). [15]

Secondly, although the study covers several years, the period is still too short to fully capture long-term trends, especially in a context where there is significant year-to-year variability (weather anomalies, changes in land use, etc.). It is therefore essential to interpret the trends identified by the Mann-Kendall test with caution, considering them as preliminary indicators rather than definitively confirmed changes.

In addition, uncertainties associated with TROPOMI products (cloud cover conditions, rendering issues near steep terrain, quality criteria) may influence certain periods or specific areas of the region. The use of monthly or annual averages, while facilitating analysis, also tends to smooth out extreme values and minimize episodes of intense pollution. Finally, the research focused on a limited group of gaseous pollutants (CO, NO_2, SO_2, O_3, CH_4) and does not yet include fine particulate matter (PM_{10}, $PM_{2.5}$), which is crucial for a comprehensive assessment of the health effects of air pollution.

Although these limitations exist, this research represents a significant step forward in understanding air pollution in the Itasy region and opens up many avenues for further study. A first approach would be to extend the time series to include future years, with the aim of consolidating the robustness of the observed trends and assessing the possible effect of changes in practices (urban expansion, agricultural transformations, controlled fire regulation, etc.). The inclusion of data from other detectors (such as those specific to aerosols or fine particles) could also help to broaden the range of pollutants analyzed.

Another important perspective focuses on the complementarity between satellite observations and in situ measurements. The establishment of certain reference stations (fixed stations or micro-sensors) in representative locations (urban, rural, near major roads) would make it possible to confirm satellite measurements, refine uncertainties, and obtain data with high temporal resolution (hourly or daily).

Finally, the approach developed in the Itasy region could be extended to other regions of Madagascar in order to compare pollution profiles, identify the most vulnerable areas, and provide decision-making support for public policies on air quality and environmental health.

5 CONCLUSION

The study highlighted several key points. NO_2 and CO concentrations in the atmospheric column follow a marked annual cycle, with maxima during the dry season (July-October) and minima during the wet season. Similarly, tropospheric ozone is higher at the end of the dry season due to strong sunlight and an abundance of precursors (NO_x, CO). In contrast, sulfur dioxide (SO_2) remains very low on average, with no clear seasonal peak. From a spatial perspective, the average maps reveal that the highest levels of CO, NO_2, and O_3 are concentrated around urban areas and major roads (Arivonimamo, Miarinarivo), while rural areas have lower concentrations (except for CH_4 linked to agricultural activities). Methane (CH_4) shows a clear upward trend (Kendall's coefficient $\tau = 0.74$, Sen slope plus or minus 10.6 ppb/year), suggesting a gradual increase in CH_4 background levels in the region, probably due to agricultural sources and combustion emissions. The temporal and spatial profiles observed confirm that anthropogenic emissions and seasonal fires dominate local air pollution, particularly during the dry season. These results represent a significant advance in understanding air pollution in tropical rural areas.

The use of Sentinel-5P/TROPOMI data has proven useful for monitoring pollutant dynamics on a global scale, complementing existing climate data. However, several limitations should be noted. The study is based primarily on satellite data with relatively coarse spatial resolution (approximately 1 km), which does not allow for the capture of very local variations (e.g., along roads or near combustion points). In addition, the period analyzed (2019-2024) is still too short to establish definitive climate trends. TROPOMI products may contain uncertainties (cloud cover, terrain restitution, quality criteria), and the use of monthly averages mitigates daily variations and pollution peaks. Finally, this work focuses on tracer gases and does not take into account fine particles (PM_{10}, $PM_{2.5}$), which are essential for assessing the overall health impact of pollution. Despite these limitations, this study opens up several possibilities, as the addition of sensors dedicated to aerosols and fine particles would broaden the range of pollutants monitored. Complementarity with in situ measurements (fixed stations or microsensors placed in representative urban and rural sites) would enable satellite data to be validated and refined. Finally, the approach developed in Itasy could be extended to other regions of Madagascar in order to compare pollution profiles and identify the most vulnerable areas, thereby guiding public policy on air quality and environmental health.

REFERENCES

[1] W. Bank, MADAGASCAR Country Environnemental Analysis, Statistics on air pollution in Antananarivo, MEDD, 2022.

[2] W. bank, Madagascar CCDR, Background Note Climate-Smart Agriculture, 2024.

[3] S. Online, Sentinel-5 Precursor Level 2 Nitrogen Dioxide, 2018.

[4] C. Thomas Brinkhoff, Analamanga Region in Madagascar, 2020.

[5] M. /. INSTAT, Monographie de la Région Itasy,, Ministère de l'Agriculture, de l'Élevage et de la Pêche, Antananarivo., 2004.

[6] W. M. Organization, World Weather Information Service, 2025.

[7] H. B. B. B. P. e. a. Hersbach, Température - ERA5 Monthly. The ERA5 global reanalysis, vol. 146(730), Quarterly Journal of the Royal Meteorological Society.

[8] T. Pohlert, Non-Parametric Trend Tests and Change-Point Detection. R package 'trend' vignette., Guide pratique très cité pour l'usage du MK dans les séries environnementales, 2023.

[9] D. H. a. R. Hirsch, Statistical Methods in Water Resources, U.S. Geological Survey Techniques, 2002.

[10] R. M. H. A. J. R. SLACK, A Nonparametric Trend Test for Seasonal Data With Serial Dependence, vol. 20, WATER RESOURCES RESEARCH,, 1984, pp. 727-732.

[11] J. C. J. H. Y. &. C. I. Benesty, Pearson correlation coefficient. In: Noise reduction in speech processing, Springer, Berlin, Heidelberg, 2009, p. p. 1-4..

[12] R. Gilbert, Statistical Methods for Environmental Pollution Monitoring., Van Nostrand Reinhold, New York, 1987.

[13] H. Theil, A rank-invariant method of linear and polynomial regression analysis, Vols. %1 sur %2 53,, Nederl. Akad. Wetensch. Proc, 1950, p. 386-392.

[14] Mongabay, Top environment stories from Madagascar in 2020, 2020.

[15] R. V. ,. Martin, Satellite remote sensing of surface air quality. Atmospheric Environment, vol. 42(34), 2008.